

## Heavy-Ion Physics Results from CMS

GÁBOR I. VERES<sup>(1)</sup> (\*)

<sup>(1)</sup> *CERN - European Organization for Nuclear Research*

**Summary.** — This paper summarizes recent experimental results related to heavy-ion collisions from the CMS Collaboration. Global features, like charged particle and transverse-energy density as a function of pseudorapidity, as well as correlations, elliptic flow, and the production of hard probes like isolated photons,  $Z$  and  $W$  bosons, jets,  $J/\psi$  and  $\Upsilon$  particles will be presented. Many of these observations are possible for the first time at the LHC, and the CMS experimental apparatus is well suited to conduct detailed studies of hard probes in the recently collected high-luminosity Pb+Pb data.

PACS 25.75.-q – Relativistic heavy-ion collisions.

PACS 25.75.Ag – Global features in relativistic heavy-ion collisions.

PACS 25.75.Bh – Hard scattering in relativistic heavy-ion collisions.

PACS 25.75.Cj – Photon, lepton, and heavy quark production in relat. HI coll.

PACS 25.75.Gz – Particle correlations and fluctuations.

PACS 25.75.Ld – Collective flow.

### 1. – Introduction

The strong interaction – described by the theory of Quantum Chromodynamics, QCD – is one of the fundamental forces in Nature. At the extremely high energy density of about  $1 \text{ GeV}/\text{fm}^3$  and at a temperature of  $150\text{--}180 \text{ MeV}/k_B$ , the nuclear matter is predicted to undergo a phase transition, beyond which the relevant degrees of freedom are the quarks and gluons. The only available experimental tools to create these conditions in the laboratory are the collisions of heavy ions, such as Pb nuclei. The present paper is a brief overview of recent results from the CMS Collaboration at the Large Hadron Collider (LHC), based on the first two heavy-ion data-taking periods in 2010 and 2011.

The first indications of the QCD phase transition appeared at the CERN SPS accelerator. The Relativistic Heavy Ion Collider (RHIC) has extended the experimental investigations at the center-of-mass energy per nucleon pair of  $\sqrt{s_{NN}} = 0.2 \text{ TeV}$ . At the LHC, in PbPb collisions at  $\sqrt{s_{NN}} = 2.76 \text{ TeV}$  it has become possible to use fully

---

(\*) On leave from the Eötvös Loránd University, Budapest

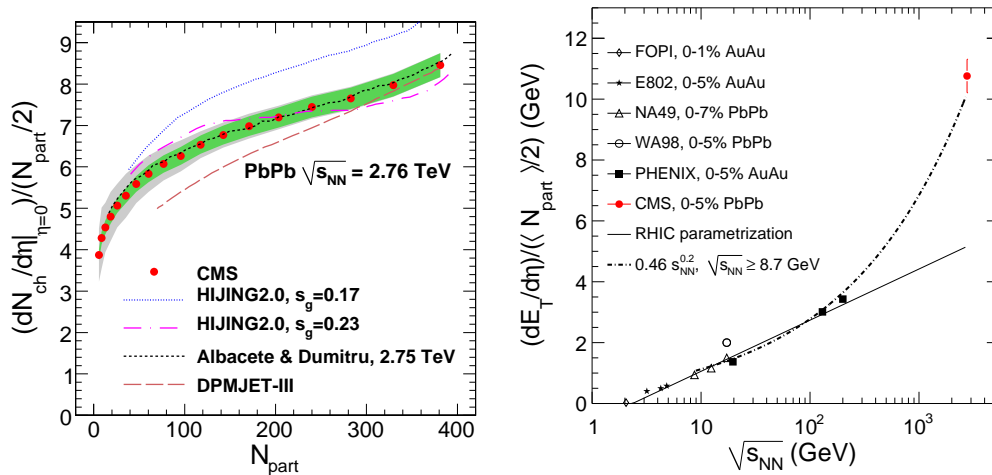


Fig. 1. – Left: Normalized charged particle density,  $dN_{ch}/d\eta/(N_{part}/2)$ , compared with model predictions [1, 2, 3] as a function of the number of participants,  $N_{part}$ , in 2.76 TeV PbPb collisions. Right: Normalized transverse-energy density for central collisions at  $\eta = 0$  as a function of the center-of-mass energy, compared to data at lower  $\sqrt{s_{NN}}$ .

reconstructed energetic jets,  $Z$  and  $W$  bosons, isolated high- $p_T$  photons, and  $\Upsilon$  mesons, so-called ‘hard probes’ to study the characteristics of the high energy density medium.

The CMS detector is well adapted to measure these hard probes, with its strong, 3.8 T magnetic field, electromagnetic and hadronic calorimeters covering a large pseudorapidity range  $|\eta| < 5.2$ , high-precision silicon tracking system ( $|\eta| < 2.4$ ), large muon detectors outside the superconducting solenoid and the calorimeter layers and the flexible, two-level trigger system [4]. At very small angles with respect to the beam line, the CASTOR calorimeter and the Zero Degree Calorimeters (ZDCs) complement the central apparatus.

The high center-of-mass energy and the experimental capabilities make it possible to study a variety of observables, among them the  $\eta$ -distributions of charged particles and transverse energy; the Fourier-spectrum of single-particle azimuthal-angle distributions and two-particle correlations; electroweak ‘candles’ like isolated photons and the  $Z$  and  $W$  bosons. Furthermore, the good dimuon-mass resolution allows one to reconstruct the members of the  $J/\psi$  and  $\Upsilon$  families separately. Finally, various aspects of the energy loss of hard-scattered partons as they traverse the created medium can be studied: the suppression of high- $p_T$  charged particles, the  $p_T$ -imbalance of reconstructed jet pairs as a function of  $p_T$  and centrality, and a comparison of jet fragmentation functions in PbPb and pp collisions. Many of these results already utilize the data set collected in 2011.

## 2. – Bulk observables

The CMS apparatus is capable of detecting particles in a very wide kinematic range. At the low transverse momentum end, charged hadrons down to  $p_T \approx 30$  MeV/c have been measured without magnetic field with the pixel layers of the inner tracker system. Simple counting of pixel clusters and reconstructing two-point tracklets were in agreement at the percent level. The measured number of charged particles per unit of pseudorapidity is normalized by the number of nucleons participating in the collision according to the Glauber-model,  $N_{part}$ , in each centrality class. The results can be seen in the left panel of

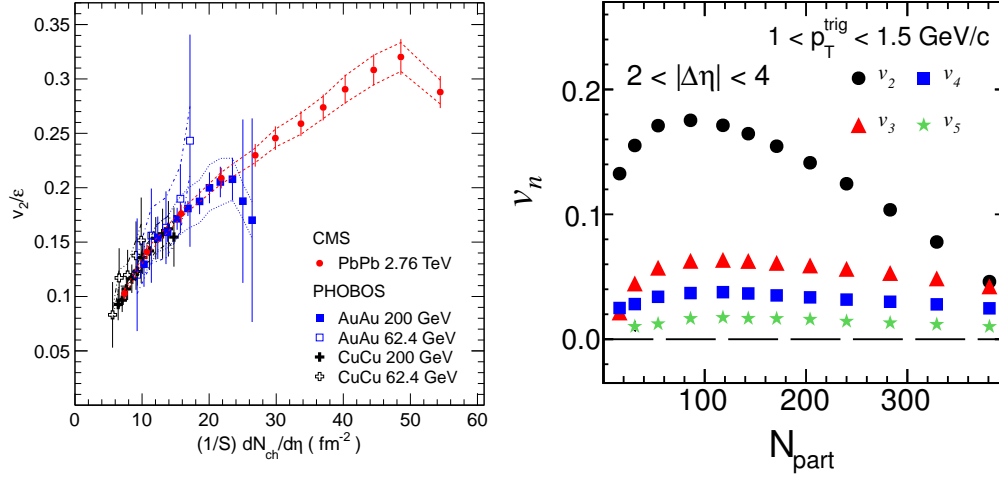


Fig. 2. – Left: Eccentricity-scaled  $v_2$  as a function of charged particle density from CMS and PHOBOS. The error bars include both statistical and systematic uncertainties of  $v_2$ . The dashed lines represent the systematic uncertainties in the eccentricity determination. Right: The single-particle azimuthal anisotropy harmonics,  $v_2 - v_5$ , extracted from the long-range ( $2 < |\Delta\eta| < 4$ ) azimuthal dihadron correlations as a function of  $N_{part}$  in PbPb collisions at  $\sqrt{s} = 2.76$  TeV for  $1 < p_T^{assoc} < 3$  GeV/c and  $1 < p_T^{trig} < 1.5$  GeV/c.

fig. 1 [5], compared to various model predictions, including the HIJING event generator with two different gluon shadowing parameters [1], a calculation based on the gluon saturation approach [2], and the DPMJET-III model [3]. The number of particles created in the collision per participant nucleon increases with the total volume of the overlap zone, and the measured particle densities provide constraints on the initial conditions of the quark-gluon matter in any hydrodynamical approach.

The wide pseudorapidity coverage of the CMS calorimeters can be utilized to measure the transverse energy produced in heavy-ion collisions, after corrections for calorimeter energy scale, acceptance, and low-energy particles deflected by the magnetic field.

The collision energy dependence of the normalized transverse-energy distribution,  $(dE_T/d\eta)/(\langle N_{part} \rangle/2)$  is plotted in the right panel of fig.1 for central PbPb collisions at  $\eta = 0$ . Between the RHIC and LHC energies, the amount of transverse energy created in the collision increases more quickly than the logarithm of  $s_{NN}$  used to describe data at lower energies. Similarly to the charged particle multiplicity, the energy dependence is better described by  $s_{NN}^n$  with  $n \approx 2$ . Between the top RHIC and LHC energies, the normalized transverse-energy density increases by a factor of  $3.3 \pm 0.3$ , while the same increase for the charged particle multiplicity is only  $2.35 \pm 0.15$  [11].

The energy density per unit volume in a central PbPb collision is estimated using the Bjorken-formula [12] to be  $15 \text{ GeV}/\text{fm}^3$ , for a formation time of  $1 \text{ fm}/c$  and transverse radius of  $7 \text{ fm}$ , which is hundred times more than the normal nuclear density.

The azimuthal anisotropy of the final state charged particles, characterized by the second Fourier coefficient,  $v_2$ , was measured as a function of  $p_T$ ,  $\eta$  and centrality using various methods. The  $v_2/\epsilon$  ratio, where  $\epsilon$  is the initial geometrical eccentricity of the set of interacting (participating) nucleons, is expected to scale with the charged particle density normalized by the transverse overlap area. Indeed, the left panel of fig. 2 shows that the relation between the two quantities, that is thought to be related to the shear viscosity to the entropy density ratio of the hydrodynamically evolving system, does not

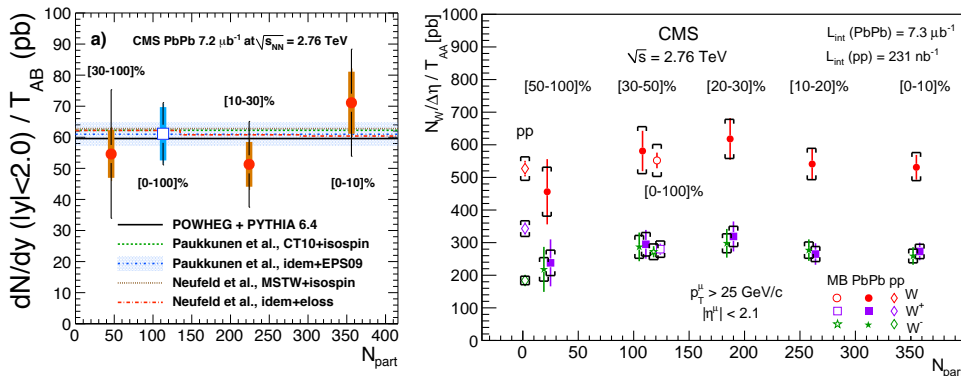


Fig. 3. – Left: The  $dN/dy$  of  $Z \rightarrow \mu^+\mu^-$  per event divided by the nuclear overlap function  $T_{AB}$  as a function of  $N_{part}$ , compared to theoretical predictions [6, 7, 8, 9, 10]. Right: Centrality dependence of the  $W^\pm \rightarrow \mu^\pm\nu$  yields in PbPb and pp collisions. Yields are given for events where the muon falls in the region  $|\eta| < 2.1$  and  $p_T > 25 \text{ GeV}/c$ .

depend on the collision energy between  $\sqrt{s_{NN}} = 62.4$  and  $2760 \text{ GeV}$  [13].

Asymmetries in the azimuthal angle ( $\phi$ ) distributions of single particles lead to non-uniform  $\Delta\phi$  distributions of particle pairs. If the two particles are distant in terms of pseudorapidity, the latter can be derived from the single-particle distributions using a simple factorization. This observation allows for the extraction of the Fourier-coefficients,  $v_2 - v_5$  of the single-particle distributions from long-range ( $2 < |\Delta\eta| < 4$ ) two-particle correlations [14]. These coefficients measured in a given  $p_T$  bin of selected particle pairs is presented in the right panel of fig. 2.

### 3. – Hard probes

Hard scattering processes creating electroweak bosons play an important reference role in the heavy-ion research at LHC, because these particles ( $\gamma$ ,  $Z$ ,  $W$ ) can be observed without modification by the strongly interacting colored medium. Measurements of the cross sections of isolated photons at high  $p_T$  [15], as well as  $Z \rightarrow \mu^+\mu^-$  [16] and  $W^\pm \rightarrow \mu^\pm\nu$  [17] processes in PbPb collisions were completed using the CMS electromagnetic calorimeters, tracker and muon systems and the capabilities of measuring the missing transverse momentum, respectively. The production yields of these three particles, normalized by the nuclear overlap function, is consistent with that measured or calculated for pp collisions at the same center-of-mass energy, as can be seen in fig. 3 and fig. 5. Different yields of  $W^+$  and  $W^-$  particles were observed in PbPb with respect to that in pp collisions, reflecting the different  $u$  and  $d$  quark content in the proton and neutron and the  $Z/A$  ratio of the Pb ion.

The good momentum resolution and precise vertexing capabilities of the CMS tracking system make it possible to statistically separate the promptly produced  $J/\psi$  particles, observed via their dimuon decay, from those originating from b-hadron decays, based on the decay length distribution [18]. These particles are expected to be suppressed in a high-temperature environment due to Debye-screening, as a direct consequence of deconfinement. The  $J/\psi$  yield, normalized by the nuclear overlap function and the yield measured in pp collisions, which is called the nuclear modification factor,  $R_{AA}$ , is presented on the left panel of fig. 4 as a function of  $N_{part}$ . The strongest suppression

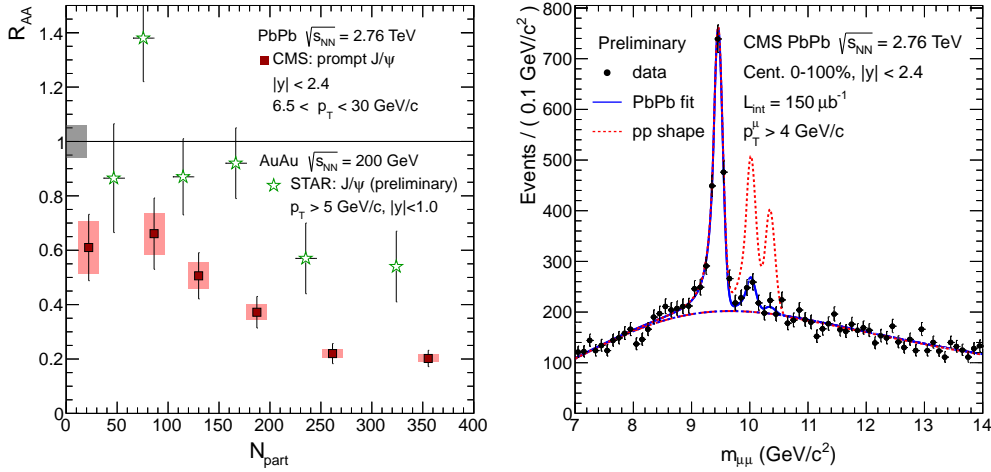


Fig. 4. – Left:  $R_{AA}$  of prompt  $J/\psi$  vs.  $N_{part}$  compared to STAR. Right: Dimuon invariant-mass distribution from the PbPb data at  $\sqrt{s_{NN}} = 2.76$  TeV. The blue solid line shows the fit to the PbPb data. The red dashed line shows the shape obtained from the fit to the pp data.

is observed in central PbPb events, exceeding that measured at RHIC in a somewhat different  $p_T$  and  $\eta$  range.

The other spectacular observation of quarkonium suppression is illustrated in the right panel of fig. 4, where the  $\Upsilon(1S)$ ,  $\Upsilon(2S)$  and  $\Upsilon(3S)$  mass peaks are shown in the  $\mu^+\mu^-$  invariant mass distribution for both PbPb and pp collisions, with the  $\Upsilon(1S)$  yields normalized between the two systems. In PbPb events the excited  $\Upsilon$  states are suppressed with respect to pp collisions, leading to a similar interpretation as for the  $J/\psi$  particles.

Summarizing the present knowledge on the single particle suppression, we can conclude that the production of charged hadrons [19] and  $J/\psi$  particles created from b-quark decays are strongly suppressed in central PbPb collisions compared to the pp reference, as demonstrated in fig. 5. The left panel compares the CMS measurement of charged particle  $R_{AA}$ , extending to  $p_T = 100$  GeV/c to lower energy data and various model predictions [20, 21, 22, 23, 24, 25], while the right panel summarizes the results on  $\gamma$ ,  $Z$ , and  $W$  production, including  $b$  quarks [15, 16, 17, 18, 19].

The suppression of particle production at a given  $p_T$  is thought to be a consequence of the steeply decreasing  $p_T$  distribution of particles combined with the energy loss of hard-scattered partons which fragment into hadrons, as they traverse the hot and dense medium created in the heavy-ion collision. Since this medium inherits an elongated geometrical shape from the nuclear overlap zone in the plane perpendicular to the beam line, the azimuthal asymmetry of high- $p_T$  hadrons should be sensitive to the above mentioned energy loss as a function of path length covered in the hot plasma. Most of the high- $p_T$  hadrons originate from the fragmentation of energetic jets, and thus their azimuthal asymmetry stems from completely different physical processes compared to low  $p_T$ , where the hydrodynamical evolution of the system plays a key role.

The flexibility of the CMS trigger system allowed for the design and utilization of a unique high- $p_T$  trigger, which selects events that contain a charged particle in the tracker system above a given  $p_T$ -threshold. Sufficient number of such collisions were recorded to make the measurement of the  $v_2$  Fourier-coefficient possible up to  $p_T \approx 60$  GeV/c [26]. The result is presented in fig. 6 as a function of  $p_T$  in six centrality classes, proving that the azimuthal asymmetry stays larger than zero up to about 40 GeV/c.

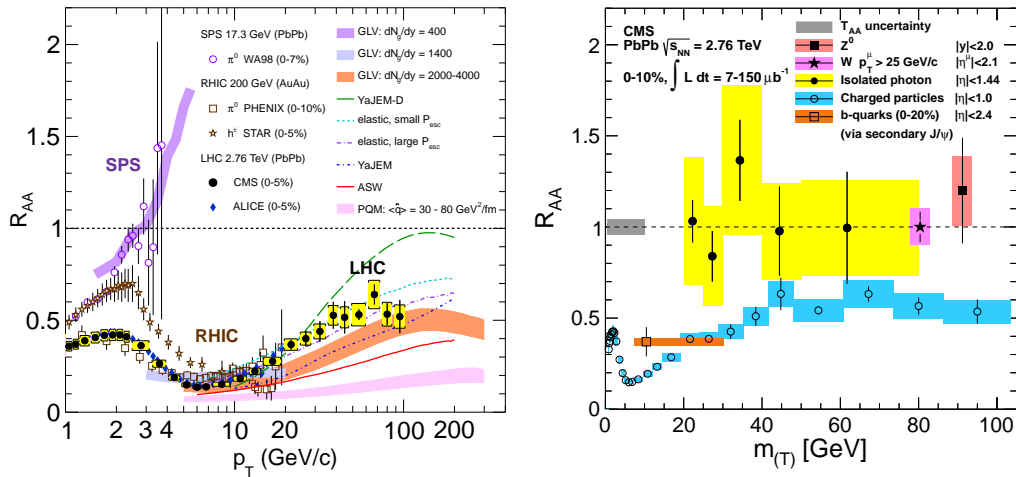


Fig. 5. – Left: The nuclear modification factor  $R_{AA}$  in central heavy-ion collisions at three different center-of-mass energies, as a function of  $p_T$ , for neutral pions and charged hadrons, compared to theoretical predictions [20, 21, 22, 23, 24, 25]. Right:  $R_{AA}$  for charged particles in central collisions, along with  $R_{AA}$  measurements for photons,  $Z$ ,  $W$  and non-prompt  $J/\psi$  particles. For the  $Z$  and  $W$  results, the data point is plotted at the rest mass of the particle, otherwise they are plotted at the  $m_T = \sqrt{m^2 + p_T^2}$  (transverse mass) value. For charged hadrons, pion mass is assumed.

The CMS calorimeter and tracking system is highly segmented and has a wide  $\eta$ -coverage, and capable to deliver enough detail for jet reconstruction even in the high multiplicity environment of central PbPb collisions. The energy contribution from the underlying event is subtracted using a suitably designed algorithm [27]. This way, experimental investigations of the parton energy loss can be taken to the next, deeper level, bypassing the complications of the jet fragmentation process. Large imbalance between the transverse momenta of the fully reconstructed leading (highest- $p_T$ ) and subleading (second highest  $p_T$ ) jets was observed, as compared to pp collisions, which is the direct consequence of parton energy loss in the medium. The mean transverse-momentum ratio,  $\langle p_{T,2}/p_{T,1} \rangle$ , of subleading and leading jets reconstructed back-to-back in azimuth (requiring  $\Delta\Phi_{1,2} > 2\pi/3$ ), is plotted in fig. 7, as a function of the transverse momentum of the leading jet,  $p_{T,1}$ , in three centrality classes. With increasing centrality, the imbalance grows, while the difference between the measured ratio in PbPb collisions and the reference (pp simulation embedded in simulated heavy-ion events) is independent of transverse momentum. On the other hand, the sharp back-to-back correlation of the leading and subleading jet in azimuthal angle, similar to jets in pp collisions, is preserved also in PbPb collisions.

The CMS Collaboration investigated several further aspects of the jet momentum imbalance. The momentum missing from the cone of the subleading jet was found back, carried by low- $p_T$  particles and by particles outside of the jet cone [28]. Furthermore, jet fragmentation functions were studied and compared between heavy-ion and pp collisions, and the hard part of the fragmentation pattern was found to be remarkably similar between jets created in the medium and those propagating in vacuum [29], independently of the imbalance between the two jets. Recently, further evidence for parton energy loss was presented in form of the momentum imbalance of  $\gamma$ -jet events [30]. The high

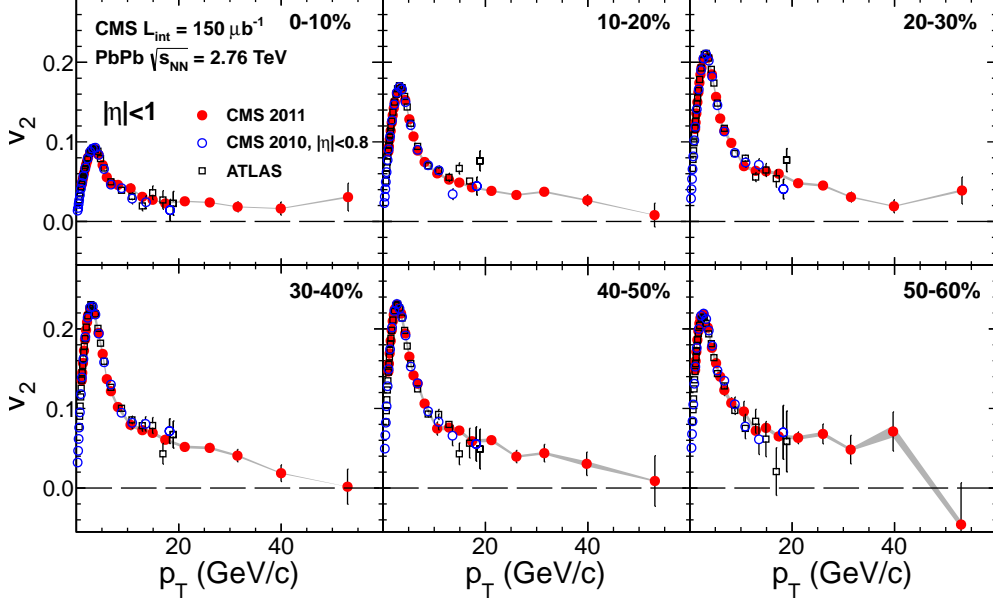


Fig. 6. – The anisotropy harmonics,  $v_2$ , as a function of  $p_T$  for six centrality ranges in PbPb collisions at  $\sqrt{s_{NN}} = 2.76$  TeV, measured by the CMS experiment (solid markers). Comparison to results from the ATLAS (open squares) and CMS (open circles) experiments using data collected in 2010 is also shown.

energy frontier at the LHC has clearly opened up a new set of possibilities to carry out detailed studies of the strongly interacting matter in an extended volume under extreme conditions.

#### 4. – Summary

The CMS experiment has measured the particle and transverse-energy density created in heavy-ion collisions, indicating the presence of strongly interacting medium with an extremely high energy density, and various effects of collective motion, influenced by the geometrical asymmetries of the initial nuclear overlap zone at the moment of the collision. It was shown that the high- $p_T$  photons,  $Z$  and  $W$  bosons are not modified by the strongly interacting medium created in high-energy heavy-ion collisions. These measurements served as the first steps of the first gamma-jet correlation study at the LHC. On the other hand, a strong suppression of charged hadrons,  $J/\psi$  and  $\Upsilon$  particles and their excited states was observed. The  $J/\psi$  mesons originating from b-quark decays were separated from the prompt ones, and an indirect evidence for b-quark energy loss was provided. The transverse-momentum imbalance of dijet events was studied in detail, indicating a strong parton energy loss in the medium, with no significant modification of the angular correlation between the jets. The momentum imbalance of jets is compensated by low- $p_T$  particles over a large spread in angle with respect to the jet axis, while the fragmentation functions observed in PbPb and pp collisions are similar, and independent of the parton energy loss.

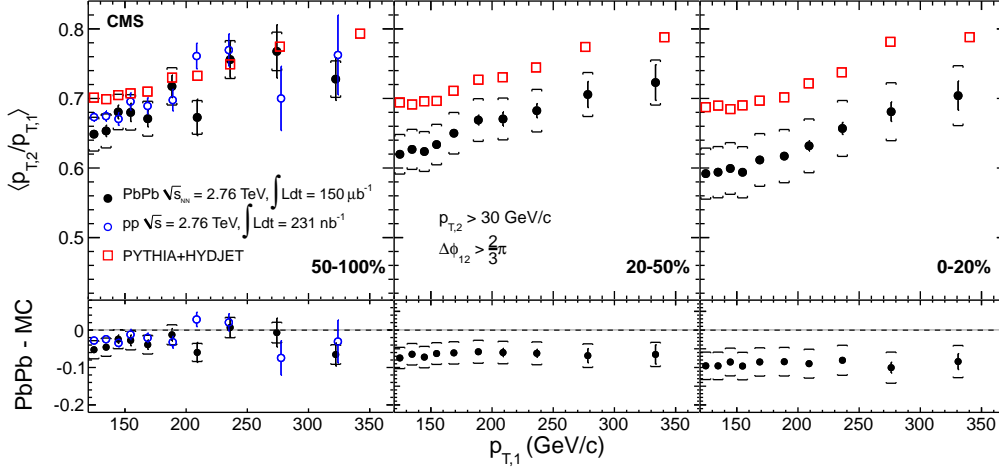


Fig. 7. – Average dijet momentum ratio,  $\langle p_{T,2}/p_{T,1} \rangle$ , as a function of leading jet  $p_T$  for three bins of collision centrality. PbPb data are shown as points, while predictions from the PYTHIA+HYDJET model are shown as squares. In the most peripheral bin, results are compared with pp data (open circles). The difference between the PbPb measurement and the expectations from PYTHIA+HYDJET is shown in the bottom panels.

#### REFERENCES

- [1] W.-T. Deng, X.-N. Wang and R. Xu, *Phys. Lett. B*, **701** (2011) 133
- [2] J. L. Albacete and A. Dumitru, *arXiv:1101.5161*, [**hep-ph**] (2011)
- [3] F. W. Bopp, R. Engel, J. Ranft and S. Roesler, *arXiv:0706.3875*, [**hep-ph**] (2007)
- [4] S. Chatrchyan *et al.* [CMS Collaboration], *JINST*, **3** (2008) S08004
- [5] S. Chatrchyan *et al.* [CMS Collaboration], *JHEP*, **1108** (2011) 141
- [6] H. Paukkunen and C. A. Salgado, *JHEP*, **1103** (2011) 071
- [7] K. J. Eskola, H. Paukkunen and C. A. Salgado, *JHEP*, **0904** (2009) 065
- [8] R. B. Neufeld, I. Vitev and B. W. Zhang *Phys. Rev. C*, **83** (2011) 034902
- [9] A. Martin, W. Stirling and R. Thorne *Eur. Phys. J. C*, **63** (2009) 189
- [10] S. Alioli, P. Nason, C. Oleari *et al.* *JHEP*, **0807** (2008) 060
- [11] S. Chatrchyan *et al.* [CMS Collaboration],
- [12] J. D. Bjorken *et al.* [CMS Collaboration], *Phys. Rev. D*, **27** (1983) 140
- [13] S. Chatrchyan *et al.* [CMS Collaboration], *arXiv:1204.1409*, [**nucl-ex**] (2012)
- [14] S. Chatrchyan *et al.* [CMS Collaboration], *arXiv:1201.3158*, [**nucl-ex**] (2012)
- [15] S. Chatrchyan *et al.* [CMS Collaboration], *Phys. Lett. B*, **710** (2012) 256
- [16] S. Chatrchyan *et al.* [CMS Collaboration], *Phys. Rev. Lett.*, **106** (2011) 212301
- [17] S. Chatrchyan *et al.* [CMS Collaboration], *arXiv:1205.6334*, [**nucl-ex**] (2012)
- [18] S. Chatrchyan *et al.* [CMS Collaboration], *JHEP*, **1205** (2012) 063
- [19] S. Chatrchyan *et al.* [CMS Collaboration], *Eur. Phys. J. C*, **72** (2012) 1945
- [20] A. Dainese, C. Loizides, G. Paic, *Eur. Phys. J. C*, **38** (2005) 461
- [21] I. Vitev and M. Gyulassy, *Phys. Rev. Lett.*, **89** (2002) 252301
- [22] I. Vitev, *J. Phys. G*, **30** (2004) S791
- [23] C. A. Salgado and U. A. Wiedemann, *Phys. Rev. D*, **68** (2003) 014008
- [24] N. Armesto, A. Dainese, C. A. Salgado *et al.*, *Phys. Rev. D*, **71** (2005) 054027
- [25] T. Renk *et al.*, *Phys. Rev. C*, **84** (2011) 014906
- [26] S. Chatrchyan *et al.* [CMS Collaboration], *arXiv:1204.1850*, [**nucl-ex**] (2012)
- [27] S. Chatrchyan *et al.* [CMS Collaboration], *Phys. Lett. B*, **712** (2012) 176
- [28] S. Chatrchyan *et al.* [CMS Collaboration], *Phys. Rev. C*, **84** (2011) 024906
- [29] S. Chatrchyan *et al.* [CMS Collaboration], *arXiv:1205.5872*, [**nucl-ex**] (2012)
- [30] S. Chatrchyan *et al.* [CMS Collaboration], *arXiv:1205.0206*, [**nucl-ex**] (2012)